AIAA SciTech Forum
8-12 January 2024, Orlando, FL
AIAA SCITECH 2024 Forum

10.2514/6.2024-1589

Control Synthesis for a Hypersonic Vehicle with Harmonic Excitation Inputs and Input-Output-Sampled Nonlinearities

Sze Kwan Cheah*, Diganta Bhattacharjee†, Maziar S. Hemati‡, and Ryan J. Caverly§
University of Minnesota, Minneapolis, MN 55455

This paper presents a control synthesis method for the flight testing of a hypersonic vehicle. The dynamic model of a hypersonic vehicle is highly nonlinear and features terms that are the result of computational fluid dynamics simulations or data from wind tunnel testing performed across a number of operating conditions. This results in lookup-table-based models that are not analytic in nature, making it difficult to apply typical nonlinear control techniques without curve fitting, which can introduce inaccuracies. To overcome the need for curve fitting, the proposed control synthesis method uses quadratic constraints to bound the sampled nonlinear dynamics of a hypersonic vehicle for control synthesis. Sampling the nonlinear dynamics comes with the challenge of synthesizing a controller while staying within the bounds of the sampled region. This is addressed in the proposed approach through an iterative synthesis method that involves solving convex semi-definite programs. Flight tests often include harmonic inputs to excite the vehicle's dynamics for system identification and refinement purposes. A novel feature of the proposed control synthesis method is the ability to bound the vehicle's states in the presence of these harmonic excitation signals. This provides a quantification of the region of allowable initial conditions that will ensure the vehicle stays within the sampled region of the state space, as demonstrated in numerical simulation results.

I. Introduction

Hypersonic vehicles traveling at speeds greater than Mach 5 are currently under development for commercial and defense applications. Developing robust feedback controllers for these vehicles is challenging due to their highly uncertain, nonlinear, and coupled dynamics, which stems from the difficulty in capturing complex aerothermodynamics at hypersonic speeds. This is especially true for prototype hypersonic flight vehicles, where opportunities to collect flight test data to refine the vehicle model are limited and the available flight tests are limited in duration. In this scenario, it is essential to develop feedback controllers and flight maneuvers that sufficiently excite the vehicle's dynamics within a short window of time while ensuring that closed-loop stability and safety-critical constraints are maintained in the presence of relatively large model uncertainty.

Model-based control methods are found in the literature for hypersonic vehicles, notably [1], which features a robust control design and the adaptive sliding mode control proposed by [2]. While these controllers address the nonlinear dynamics of a hypersonic vehicle, they rely on knowledge of an analytic form of the system's nonlinearities, albeit while accounting for uncertainty in certain model parameters. This is a potential limitation when working with dynamic models generated from computational fluid dynamics (CFD) simulations [3] or experimental wind tunnel data [4], which typically provide modeling information at specific points within a parametric space (e.g., a lookup table of aerodynamic coefficients), rather than an analytic model. In the case of a hypersonic flight test, it may be required to design flight test controllers based on such a model, which limits the use of traditional nonlinear control approaches.

Data-driven techniques are now becoming increasingly popular within the control community to overcome these issues [5]. For example, strategies are being developed to determine the input-output properties of dynamical systems from sampled data, including identifying dissipation inequalities [6] and passivity metrics [7]. Once the input-output properties of a system or a portion of the system are identified from data, stability theorems (e.g., passivity theorem, circle criterion) can be leveraged to design controllers that ensure closed-loop stability properties. This input-output approach allows for a "black box" interpretation of the complicated, nonlinear, and possibly uncertain aspects of the system, while allowing for a framework in which stabilizing controllers can be designed.

*Ph.D. Student, Department of Aerospace Engineering and Mechanics, AIAA Student Member, email: cheah013@umn.edu.
†Postdoctoral Research Associate, Department of Aerospace Engineering and Mechanics, AIAA Member, email: dbhattac@umn.edu.
‡Associate Professor, Department of Aerospace Engineering and Mechanics, AIAA Associate Fellow, email: mhemati@umn.edu.
§Assistant Professor, Department of Aerospace Engineering and Mechanics, AIAA Member, email: rcaverly@umn.edu.

This paper makes use of data-driven input-output control theory to develop a control design method for the stabilization of a hypersonic flight test vehicle with nonlinear dynamics. Our proposed approach follows a method similar to what is described in [8], where the nonlinear and uncertain dynamics of the hypersonic vehicle are modeled as perturbations to a known linear time-invariant (LTI) linearization of the system within a linear fractional transformation (LFT) framework. Integral quadratic constraints [9] provide a means to quantify the input-output properties of an operator (e.g., a nonlinear function or a dynamic system). Static and memoryless nonlinearities can be characterized through specific classes of quadratic constraints (QCs) [9], which are a type of integral quadratic constraint that holds point-wise in time. In this work, input-output samples of the vehicle's nonlinear dynamics are used to quantify the system's nonlinearities in terms of norm bound QCs. Control synthesis is a challenge due to the fact that the perturbations are described with input-output data and the sampling range of this data is dependent on the choice of controller. This poses a problem, as the sampled-based input-output characterization of the perturbations requires a controller to be chosen *a priori*, while a controller cannot be synthesized until this input-output characterization is known. The causality dilemma is resolved by first prescribing a closed set for the states and inputs for use in sampling and subsequent characterization of QC properties of the nonlinearities. By constraining the maximum singular value of the controller during synthesis, this ensures that the control inputs always remain within the prescribed range of sampled inputs. As the synthesis problem is non-convex, it is resolved by iteratively solving three semi-definite programs (SDPs) that are obtained through convex relaxations.

The main contributions of this work in comparison to the control methodology presented in [8] include 1) the manner in which weightings and uncertainty decomposition are employed to make the hypersonic vehicle model in [10, 11] amenable to the control synthesis method in [8] and 2) the development of an analysis and synthesis framework that extends the work in [8] to account for the exogenous excitation signals relevant to a hypersonic vehicle flight test. Our proposed control synthesis method is able to account for the sampled nonlinearities of the control-oriented hypersonic model in [10] by providing a guarantee that the vehicle states remain bounded within a specified region in the presence of harmonic excitation signals [12]. The synthesized controller provides a means of performing flight test maneuvers of a nonlinear hypersonic vehicle, while adhering to safety-critical constraints. In contrast to traditional nonlinear control techniques, this control synthesis method does not require an analytic representation of the vehicle's nonlinear dynamics.

II. Preliminaries

This section presents a problem statement outlining the objectives of this work, as well as important notation used throughout the paper.

A. Problem Statement

The objective of this paper is to synthesize a static full-state feedback controller for a hypersonic vehicle that guarantees boundedness of the system states within a prescribed region given input-output sampled bounds on the nonlinearities of the vehicle's dynamic model within the same prescribed region. The controller is also required to provide boundedness guarantees in the presence of harmonic excitation signals that would be present in a flight test.

It is worth nothing that in [10], the "truth model" was developed by [11] using physics-based first principles. There were significant differences in the drag and lift plots when comparing the truth model to the "full fit" and "simplified fit" models. The truth model is not publicly available, but the control-oriented model and associated coefficients are published in [10], allowing us to demonstrate how sampled data, not just analytic curve-fitted data can be incorporated into the control synthesis procedure.

B. Notation

The symbol $\mathcal{N}_n$ is a shorthand for the set $\{1, 2, \ldots, n\}$. The matrix of zeros and identity matrix are respectively written as $\mathbf{0}$ and $\mathbf{1}$. A column matrix of zeros with the i^{th} entry of 1 is denoted as $\mathbf{1}_i$. Matrices and vectors are represented in bold (e.g., $\mathbf{A} \in \mathbb{R}^{n\times m}$) with matrices capitalized. Symmetric n by n matrices are represented by $\mathbf{A} \in \mathbb{S}^n$, and their positive or negative definiteness is denoted by > 0 or < 0, respectively. The maximum singular value of $\mathbf{A}$ is denoted by $\overline{\sigma}(\mathbf{A})$. A given ellipsoid centered at the origin is denoted as $\mathcal{E}_n(\mathbf{E}) = \{\mathbf{x} \in \mathbb{R}^n \,|\, \left\|\mathbf{E}^{-1}\mathbf{x}\right\|_2 \leq 1\}$ and $\mathcal{B}_n$ denotes the closed unit-norm ball of radius r in $\mathbb{R}^n$.

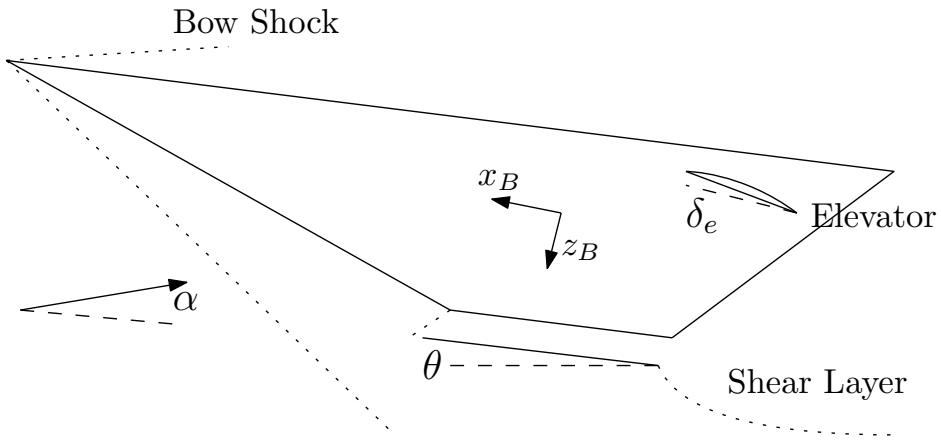

Fig. 1 Schematic of the longitudinal hypersonic model in [10]

III. Hypersonic Model Dynamics

This section presents a slightly modified version of the control-oriented hypersonic model from [10] and reformulates the dynamics to a form that is amenable to the proposed control synthesis approach. The harmonic excitation signals used as part of a flight test are also described and formulated in a manner that they can be incorporated within the hypersonic model and accounted for within the control synthesis procedure.

A. Modified Control-Oriented Model

The hypersonic vehicle model considered in this paper is based on a longitudinal Control-Oriented Model described in [10] with a minor modification by removing the engine dynamics. The nonlinear equations of motion of the hypersonic vehicle are

$$\dot{V} = \frac{1}{m}\left[T(\alpha,\Phi)\cos\alpha - D(V,\alpha)\right] - g\sin(\theta-\alpha), \tag{1}$$

$$\dot{\alpha} = \frac{1}{mV}\left[-T(\alpha,\Phi)\sin\alpha - L(\alpha)\right] + Q + \frac{g}{V}\cos(\theta-\alpha), \tag{2}$$

$$\dot{\theta} = Q, \tag{3}$$

$$\dot{Q} = \frac{1}{I_{yy}}M(V,\alpha,\delta_e,\Phi), \tag{4}$$

where V is the vehicle's velocity, α is the vehicle's angle of attack, θ is the vehicle's pitch angle, and Q is the vehicle's pitch rate. The vehicle's mass is given by m, while its moment of inertia about the pitch axis is I_{yy}. The control inputs are specified as the elevator deflection δ_e and the fuel-to-air ratio Φ. The thrust, drag, lift, and moment acting on the vehicle are nonlinear functions of the state and input, and are denoted as $T(\alpha,\Phi)$, $D(V,\alpha)$, $L(\alpha)$, and $M(V,\alpha,\delta_e,\Phi)$ respectively. Some of the states are illustrated in the simplified schematic of Fig. 1.

As described in [10], these nonlinear state- and input-dependent functions are obtained through compressible flow theory model that are analytically intractable. Furthermore direct application of nonlinear design methodologies, such as feedback linearization, to the truth model governing equations is not possible with implicit functions of the state and input variables. The control-oriented model is a curve fit and simplified model that was used for application of approximate feedback linearization technique.

The nonlinear dynamics described by (1) through (4) can be written in terms of the nonlinear ODE $\dot{\mathbf{x}} = \mathbf{f}(\mathbf{x},\mathbf{u})$, where the state is defined as $\mathbf{x} = [V \;\; \alpha \;\; \theta \;\; Q]^\mathsf{T}$ and the inputs are given by $\mathbf{u} = [\delta_e \;\; \Phi]^\mathsf{T}$. The system's nonlinear dynamics can be linearized about a trim point $(\mathbf{x}_0,\mathbf{u}_0)$, where $\mathbf{f}(\mathbf{x}_0,\mathbf{u}_0) = \mathbf{0}$, producing the LTI model $\mathbf{G}$ with state matrix $\mathbf{A} = \frac{\partial \mathbf{f}}{\partial \mathbf{x}}\big|_{\mathbf{x}_0,\mathbf{u}_0}$ and control matrix $\mathbf{B}_1 = \frac{\partial \mathbf{f}}{\partial \mathbf{u}}\big|_{\mathbf{x}_0,\mathbf{u}_0}$. A Taylor series expansion of $\dot{\mathbf{x}} = \mathbf{f}(\mathbf{x},\mathbf{u})$ results in

$$\delta\dot{\mathbf{x}} = \mathbf{A}\delta\mathbf{x} + \mathbf{B}_1\delta\mathbf{u} + \boldsymbol{\Delta}(\delta\mathbf{x},\delta\mathbf{u}), \tag{5}$$

where $\delta\mathbf{x} = \mathbf{x} - \mathbf{x}_0$, $\delta\mathbf{u} = \mathbf{u} - \mathbf{u}_0$, and $\boldsymbol{\Delta}(\delta\mathbf{x},\delta\mathbf{u})$ represent that nonlinear perturbations that account for the difference between the nonlinear dynamics and linearized dynamics. Note that (5) exactly represents the nonlinear model of the

hypersonic vehicle, as $\boldsymbol{\Delta}(\delta\mathbf{x}, \delta\mathbf{u})$ accounts for all discrepancies between the linear and nonlinear model. It is also worth noting that $\boldsymbol{\Delta}(\delta\mathbf{x}, \delta\mathbf{u})$ approaches zero as $\delta\mathbf{x} \to \mathbf{0}$ and $\delta\mathbf{u} \to \mathbf{0}$, as the nonlinear dynamics approach the linear dynamics in this limiting case.

The nonlinearities are separated into different input-output functions $p_i = \Delta_i(\mathbf{v}_i), i \in \mathcal{N}_{n_p}$ that can be individually characterized by sampled data. Their contributions to the nonlinear equations of motion appear via the signal $\mathbf{p} = [\Delta_1 \ \Delta_2 \ \cdots \ \Delta_{n_p}]^\mathsf{T} \in \mathbb{R}^{n_p}$, which leads to the reformulation of (5) given by

$$\delta\dot{\mathbf{x}} = \mathbf{A}\delta\mathbf{x} + \mathbf{B}_1\delta\mathbf{u} + \mathbf{B}_2\mathbf{p}, \tag{6}$$

$$p_i = \Delta_i(\mathbf{v}_i), \ i \in \mathcal{N}_{n_p}, \tag{7}$$

$$\mathbf{v}_i = \left(\mathbf{C}_i\delta\mathbf{x} + \mathbf{D}_i\delta\mathbf{u}\right), \ i \in \mathcal{N}_{n_p}, \tag{8}$$

where the matrices $\mathbf{C}_i$ and $\mathbf{D}_i$ determine the inputs to the input-output functions Δ_i. The higher order terms Δ_i may be determined in various ways. When analytical equations are available, the equation of motion may be decomposed into a vector sum of n_p equations

$$\delta\dot{\mathbf{x}} = \mathbf{f}(\mathbf{x}, \mathbf{u}) = \sum_{i=1}^{n_p} \mathbf{f}_i(\mathbf{x}, \mathbf{u}), \ i \in \mathcal{N}_{n_p}, \tag{9}$$

$$\mathbf{f}_i(\mathbf{x}, \mathbf{u}) = \mathbf{f}_i(\mathbf{x}_0, \mathbf{u}_0) + \left.\frac{\partial \mathbf{f}_i}{\partial \mathbf{x}}\right|_{(\mathbf{x}_0, \mathbf{u}_0)} \delta\mathbf{x} + \left.\frac{\partial \mathbf{f}_i}{\partial \mathbf{u}}\right|_{(\mathbf{x}_0, \mathbf{u}_0)} \delta\mathbf{u} + \Delta_i(\mathbf{x}, \mathbf{u}) \tag{10}$$

$$= \mathbf{f}_i(\mathbf{x}_0, \mathbf{u}_0) + \bar{\mathbf{A}}_i\delta\mathbf{x} + \bar{\mathbf{B}}_i\delta\mathbf{u} + \Delta_i(\mathbf{x}, \mathbf{u}). \tag{11}$$

Rearranging this equation yields a description of the nonlinearities in the form

$$\Delta_i(\mathbf{x}, \mathbf{u}) = \mathbf{f}_i(\mathbf{x}, \mathbf{u}) - \left(\bar{\mathbf{A}}_i\delta\mathbf{x} + \bar{\mathbf{B}}_i\delta\mathbf{u} + \mathbf{f}_i(\mathbf{x}_0, \mathbf{u}_0)\right). \tag{12}$$

Note that $\bar{\mathbf{A}}_i = \frac{\partial \mathbf{f}_i}{\partial \mathbf{x}}$ and $\bar{\mathbf{B}}_i = \frac{\partial \mathbf{f}_i}{\partial \mathbf{u}}$. The sum partial derivatives are the same (i.e., $\sum \mathbf{f}_i(\mathbf{x}_0, \mathbf{u}_0) = \mathbf{0}$, $\sum \bar{\mathbf{A}}_i = \mathbf{A}$ and $\sum \bar{\mathbf{B}}_i = \mathbf{B}$). When analytical equations are available, the selection of $\mathbf{f}_i, i \in \mathcal{N}_{n_p}$ can be made such that each Δ_i are dependent on the least number of state and inputs allowing for tighter linear bounds on the nonlinearity. Use of too many n_p however run the risk of untangling favorable cancellation and more computationally difficult to solve. Otherwise if experimental data, such as drag coefficient from wind tunnel testing or analytical data such as lift coefficient from CFD is available, they can be similarly incorporated as input-output data points of $\Delta_i, i \in \mathcal{N}_{n_p}$. The samples are often performed to span a grid space of sufficiently small interval and may be appended to approximate dynamics if needed. Furthermore, it is assumed that knowledge of an equilibrium point $\mathbf{x}_0$ and $\mathbf{u}_0$ as well as the linearized model $\mathbf{A}$ and $\mathbf{B}$ is available. This is similarly assumed for flight testing, as demonstrated in [12].

Assuming that a full-state measurement is available, a static controller of $\delta\mathbf{u} = \mathbf{K}\delta\mathbf{x}$ is chosen. The closed-loop equations can be written, without approximation, by substituting $\delta\mathbf{u} = \mathbf{K}\delta\mathbf{x}$ into (6), (7), and (8), yielding

$$\delta\dot{\mathbf{x}} = \mathbf{A}\delta\mathbf{x} + \mathbf{B}_1\mathbf{K}\delta\mathbf{x} + \mathbf{B}_2\mathbf{p}, \tag{13}$$

$$p_i = \Delta_i(\mathbf{v}_i), \ i \in \mathcal{N}_{n_p}, \tag{14}$$

$$\mathbf{v}_i = \left(\mathbf{C}_i\delta\mathbf{x} + \mathbf{D}_i\mathbf{K}\delta\mathbf{x}\right), \ i \in \mathcal{N}_{n_p}. \tag{15}$$

A block diagram illustrating the closed loop system is shown in Fig.2(a).

B. Harmonic Dynamics

Harmonic excitation is often used for flight testing [12] of prototype aircraft for system identifications and stability margin determination. These flight test maneuvers are executed by applying designed input time series to the aircraft control inputs. Often times, these inputs are sum of harmonic signals with unique frequencies and phase shifts designed to be mutually orthogonal both in time and in frequency domain. This harmonic excitation on the aircraft control inputs are made in addition to the system feedback controller. The feedback controller is necessary for a nominally unstable aircraft.

For stability analysis and synthesis, a harmonic excitation may be viewed as an exogenous signal in the existing robust control framework [13]; however, this approach can be conservative as the input signal could take on any frequency and phase. An alternate approach is taken here, where the harmonic signal is modeled through the use of

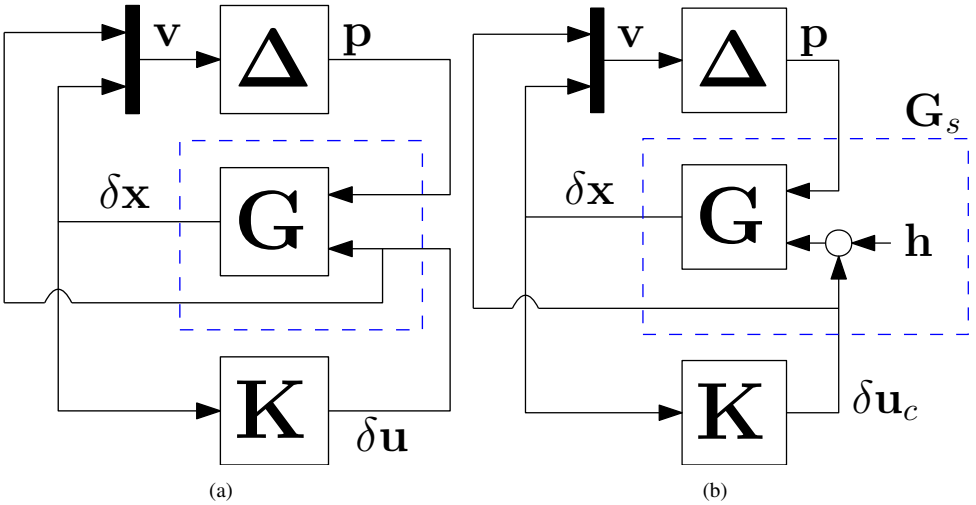

Fig. 2 Block diagrams of (a) the closed-loop nonlinear system and (b) the closed-loop nonlinear system with a harmonic excitation signal. Note that the harmonic excitation signal in (b) is modeled as the output of internal harmonic dynamics and are encapsulated within the augmented LTI system denoted as $\mathbf{G}_s$.

appended states to the original state space. Each harmonic excitation signal is represented as the free-response output of a two-state state-space system. For example, the signal $h(t) = A_1 \sin(\omega_1 + \phi_1)$ corresponds to the solution of the ordinary differential equation $\ddot{h} + 2\mu\omega_1\dot{h} + \omega_1^2 h = 0$, where $\mu = 0$ and the initial condition $\boldsymbol{\beta}_1(0)$ is chosen appropriately to match the amplitude and phase of the harmonic signal. This corresponds to the output of the state-space system

$$\dot{\boldsymbol{\beta}} = \begin{bmatrix} 0 & 1 \\ -\omega_1^2 & -2\mu\omega_1 \end{bmatrix} \boldsymbol{\beta}_1, \tag{16}$$

$$h = \begin{bmatrix} 1 & 0 \end{bmatrix} \boldsymbol{\beta}_1. \tag{17}$$

In this work, a small amount of decay or damping in the harmonic signal is introduced through the parameter $\mu > 0$ to aid with numerical computations. This damping value can be made very small to have minimal effect on the actual harmonic signal, especially for the first few cycles when flight testing is performed.

For compactness in subsequent derivations, the equations (16) and (17) are expressed as

$$\dot{\boldsymbol{\beta}}_1 = \mathbf{S}_1 \boldsymbol{\beta}_1, \tag{18}$$

$$h_1 = \mathbf{T}_1 \boldsymbol{\beta}_1, \tag{19}$$

where $\mathbf{T}_1 = \begin{bmatrix} 1 & 0 \end{bmatrix}$ and $\mathbf{S}_1 = \begin{bmatrix} 0 & 1 \\ -\omega_1^2 & -2\mu\omega_1 \end{bmatrix}$.

Now consider a signal formed by the summation of n_h harmonic signals given by

$$h = A_1 \sin(\omega_1 + \phi_1) + A_2 \sin(\omega_2 + \phi_2) + \cdots + A_{n_h} \sin(\omega_{n_h} + \phi_{n_h}). \tag{20}$$

This signal h can be generated as the output of the state-space system

$$\dot{\boldsymbol{\beta}} = \mathbf{S}\boldsymbol{\beta}, \tag{21}$$

$$h = \mathbf{T}\boldsymbol{\beta}, \tag{22}$$

where $\mathbf{S} = \text{diag}(\boldsymbol{S}_1, \boldsymbol{S}_2, \ldots \boldsymbol{S}_{n_h})$, $\mathbf{T} = [\mathbf{T}_1 \ \cdots \ \mathbf{T}_{n_h}]$ and $\boldsymbol{\beta} = [\boldsymbol{\beta}_1^\mathsf{T} \ \cdots \ \boldsymbol{\beta}_{n_h}^\mathsf{T}]^\mathsf{T}$. The states-space representation of $\mathbf{S}$ and $\mathbf{T}$ are not unique. A change of variable of variables of $\bar{\boldsymbol{\beta}} = \boldsymbol{\Pi}\boldsymbol{\beta}$ is introduced as a means to improve numerical

conditioning and weigh the effects of initial conditions that will be useful later in the control synthesis. The transformed state-space system is

$$\dot{\bar{\boldsymbol{\beta}}} = \bar{\mathbf{S}}\bar{\boldsymbol{\beta}}, \tag{23}$$

$$\mathbf{h} = \bar{\mathbf{T}}\bar{\boldsymbol{\beta}}, \tag{24}$$

where $\bar{\mathbf{S}} = \boldsymbol{\Pi}\mathbf{S}\boldsymbol{\Pi}^{-1}$, $\bar{\mathbf{T}} = \mathbf{C}_h\mathbf{T}\boldsymbol{\Pi}^{-1}$ and $\mathbf{C}_h = \mathbf{1}_c$ maps the single-dimensional harmonic signal to a column matrix whose c^{th} entry is h and all remaining entries are zero. The matrix $\mathbf{C}_h$ may be modified to incorporate more than one channel as needed.

C. Control-Oriented Model with Harmonic Excitations

The control input to the nonlinear hypersonic model described by (6), (7), and (8) is augmented with the harmonic excitation signal $\mathbf{h}$ as

$$\delta\mathbf{u} = \mathbf{K}\delta\mathbf{x} + \mathbf{h} = \mathbf{K}\delta\mathbf{x} + \bar{\mathbf{T}}\bar{\boldsymbol{\beta}} \tag{25}$$

The equation of motion in (6) can thus be rewritten as

$$\delta\dot{\mathbf{x}} = (\mathbf{A} + \mathbf{B}_1\mathbf{K})\delta\mathbf{x} + \mathbf{B}_2\mathbf{p} + \mathbf{B}_1\bar{\mathbf{T}}\bar{\boldsymbol{\beta}}. \tag{26}$$

Augmenting the state vector to include the harmonic excitation states, the new state becomes $\mathbf{z} = [\delta\mathbf{x}^\mathsf{T}\ \bar{\boldsymbol{\beta}}^\mathsf{T}]^\mathsf{T}$, which results in the augmented dynamics

$$\dot{\mathbf{z}} = \begin{bmatrix} \mathbf{A} + \mathbf{B}_1\mathbf{K} & \mathbf{B}_1\bar{\mathbf{T}} \\ \mathbf{0} & \bar{\mathbf{S}} \end{bmatrix}\mathbf{z} + \begin{bmatrix} \mathbf{B}_2 \\ \mathbf{0} \end{bmatrix}\mathbf{p} \tag{27}$$

$$= \left(\begin{bmatrix} \mathbf{A} & \mathbf{B}_1\bar{\mathbf{T}} \\ \mathbf{0} & \bar{\mathbf{S}} \end{bmatrix} + \begin{bmatrix} \mathbf{B}_1\mathbf{K} & \mathbf{0} \\ \mathbf{0} & \mathbf{0} \end{bmatrix}\right)\mathbf{z} + \begin{bmatrix} \mathbf{B}_2 \\ \mathbf{0} \end{bmatrix}\mathbf{p} \tag{28}$$

$$= (\mathbf{A}_s + \mathbf{A}_k)\mathbf{z} + \hat{\mathbf{B}}_2\mathbf{p}, \tag{29}$$

where the matrices $\mathbf{A}_s$ and $\mathbf{A}_k$ are defined to separate the portions of the dynamics that depend on the control gain $\mathbf{K}$ from those that do not.

The closed-loop equations of motion with harmonic excitation are described by

$$\dot{\mathbf{z}} = (\mathbf{A}_s + \mathbf{A}_k)\mathbf{z} + \hat{\mathbf{B}}_2\mathbf{p} \tag{30}$$

$$p_i = \Delta_i(\mathbf{v}_i),\ i \in \mathcal{N}_{n_p} \tag{31}$$

$$\mathbf{v}_i = \mathbf{E}_i\begin{bmatrix} (\mathbf{C}_i + \mathbf{D}_i\mathbf{K}) & \mathbf{D}_i\bar{\mathbf{T}} \end{bmatrix}\mathbf{z},\quad i \in \mathcal{N}_{n_p}, \tag{32}$$

where the weighting matrix $\mathbf{E}_i$ is introduced to normalize the vector $\mathbf{v}_i$ such that the norm is not greater than 1. This provide a more balanced weighting of each variable since some variables such as velocities V are much higher in amplitude compared to pitch angle θ. Setting $\mathbf{E}_i$ as a diagonal matrix with each entity being the inverse of the maximum magnitude of the corresponding state is a reasonable weighting matrix. A block diagram illustrating the closed loop system with embedded harmonic excitations is shown in Fig.2(b).

IV. Control Synthesis

The proposed control synthesis method is presented in this section, starting with a description of the linear matrix inequalities (LMI) conditions derived in [8] that guarantees closed-loop asymptotic stability of a nonlinear system with norm bounds on the system's nonlinearities. An extension of the result in [8] is then introduced as a means to provide a transient bound the norm of the state, rather than simply ensuring asymptotic stability. Matrix inequality conditions are then derived to explicitly account for harmonic excitation signals within these stability results, followed by LMI relaxations that allows for an iterative control synthesis procedure to an otherwise bilinear matrix inequality problem.

A. Control Synthesis for Closed Loop Asymptotic Stability

The proposed control synthesis method is formulated starting from the stability theorem presented in [8], which is stated in the following theorem.

Theorem IV.1. *Consider the closed-loop system described by closed-loop system described by* (13)*,* (14)*, and* (15)*, where the perturbations satisfy the norm bounds* $\|p_i\|_2 \leq \gamma_i \|\mathbf{v}_i\|_2$*,* $i \in \mathcal{N}_{n_p}$*. Let* $\mathbf{W} > 0$ *and* $r > 0$ *be chosen such that* $\mathbb{X}_c = \mathcal{E}_{n_x}(\mathbf{W}) \subseteq \mathbb{X}$ *and* $\mathbb{U}_c = r\mathcal{B}_{n_u} \subseteq \mathbb{U}$*, respectively. Then, the closed-loop system described by* (13)*,* (14)*, and* (15) *is locally asymptotically stable in* $\mathbb{X}_c$*, if there exist* $\mathbf{P} \in \mathbb{S}^{n_x}$*,* $\mathbf{K} \in \mathbb{R}^{n_u \times n_x}$*,* $\tau > 0$*, and* $\lambda_i > 0$*,* $i \in \mathcal{N}_{n_p}$*, such that* $\mathbf{P} > 0$*,*

$$\begin{bmatrix} \mathbf{P}(\mathbf{A}+\mathbf{B}_1\mathbf{K}) + (\mathbf{A}+\mathbf{B}_1\mathbf{K})^\mathsf{T}\mathbf{P} & \mathbf{P}\mathbf{B}_2 & \mathbf{\Theta} \\ \mathbf{B}_2^\mathsf{T}\mathbf{P} & \mathbf{\Lambda} & \mathbf{0} \\ \mathbf{\Theta}^\mathsf{T} & \mathbf{0} & \mathbf{\Xi} \end{bmatrix} < 0, \tag{33}$$

$$\begin{bmatrix} \tau^2\mathbf{I} & \mathbf{K} \\ \mathbf{K}^\mathsf{T} & \mathbf{W}^{-1}\mathbf{W}^{-1} \end{bmatrix} \geq 0, \tag{34}$$

$$\tau \leq r, \tag{35}$$

where $\mathbf{\Lambda} = -\mathrm{diag}\left(\lambda_1, \ldots, \lambda_{n_p}\right)$ *and* $\mathbf{\Xi} = -\mathrm{diag}(\frac{\lambda_1}{\gamma_1^2}\mathbf{I}, \ldots, \frac{\lambda_{n_p}}{\gamma_{n_p}^2}\mathbf{I}), \mathbf{\Theta} = [\lambda_1\mathbf{\Phi}_1, \ldots, \lambda_n\mathbf{\Phi}_{n_p}]$*, with* $\mathbf{\Phi}_i = \mathbf{C}_i^\mathsf{T} + \mathbf{K}^\mathsf{T}\mathbf{D}_i^\mathsf{T}$*,* $i \in \mathcal{N}_{n_p}$*.*

Proof. See proof of Theorem 3.1 in [8]. □

Theorem IV.1 provides a means to certify asymptotic stability of an autonomous nonlinear system within a local region. Although this was shown to yield a useful control synthesis method for sampled nonlinear systems in [8], it does not provide any guarantees of what might occur to the closed-loop system state during the system's transient response. For example, the state may exit the sampled region $\mathcal{E}(\mathbf{W})$ for a period of time before returning and asymptotically stabilizing to the equilibrium point. This is a limitation of Theorem IV.1 that is addressed in the following section.

B. Transient Bounds on the Closed-Loop System

LMI conditions to quantify the transient bounds on the state of an LTI system are described in [14, 15]. An extension of these results to accommodate the nonlinear closed-loop system described by (13), (14), and (15) is described in the following lemma.

Lemma IV.1. *Consider the closed-loop system described by* (13)*,* (14)*, and* (15)*, where the perturbations satisfy the norm bounds* $\|p_i\|_2 \leq \gamma_i \|\mathbf{v}_i\|_2$*,* $i \in \mathcal{N}_{n_p}$*. The transient norm bound*

$$\left\|\mathbf{W}^{-1}\delta\mathbf{x}(T)\right\|_2 \leq \xi \left\|\mathbf{W}^{-1}\delta\mathbf{x}(0)\right\|_2 \tag{36}$$

is satisfied if there exist $\mathbf{P} \in \mathbb{S}^{n_x}$ *and* $\xi \in \mathbb{R}_{>0}$ *such that* $\mathbf{P} > 0$*,* (33) *and*

$$\mathbf{W}^\mathsf{T}\mathbf{P}\mathbf{W} - \xi\mathbf{1} \leq 0, \tag{37}$$

$$\begin{bmatrix} \mathbf{W}^\mathsf{T}\mathbf{P}\mathbf{W} & \mathbf{1} \\ \mathbf{1} & \xi\mathbf{1} \end{bmatrix} \geq 0. \tag{38}$$

Proof. The non-negative function $V = \mathbf{x}^\mathsf{T}\mathbf{P}\mathbf{x}$ defined and the proof of Theorem 3.1 in [8] is used with (33) to show that $\dot{V} \leq 0$. Integrating both sides from $t = 0$ to $t = T$, where $T \in \mathbb{R}_{>0}$, yields $V(T) \leq V(0)$ or $\mathbf{x}(T)^\mathsf{T}\mathbf{P}\mathbf{x}(T) \leq \mathbf{x}(0)^\mathsf{T}\mathbf{P}\mathbf{x}(0)$. The inequality in (37) can be rewritten as $\mathbf{P} \leq \zeta\mathbf{W}^{-\mathsf{T}}\mathbf{W}^{-1}$. Applying the non-strict Schur complement to (38) results in $\mathbf{P} \geq \zeta^{-1}\mathbf{W}^{-\mathsf{T}}\mathbf{W}^{-1}$. Combining these results yields

$$\xi^{-1}\delta\mathbf{x}(T)^\mathsf{T}\mathbf{W}^{-\mathsf{T}}\mathbf{W}^{-1}\delta\mathbf{x}(T) \leq \delta\mathbf{x}(T)^\mathsf{T}\mathbf{P}\delta\mathbf{x}(T) \leq \delta\mathbf{x}(0)^\mathsf{T}\mathbf{P}\delta\mathbf{x}(0) \leq \xi\delta\mathbf{x}(0)^\mathsf{T}\mathbf{W}^{-\mathsf{T}}\mathbf{W}^{-1}\delta\mathbf{x}(0), \tag{39}$$

which proves that $\xi^{-1}\left\|\mathbf{W}^{-1}\delta\mathbf{x}(T)\right\|_2^2 \leq \xi\left\|\mathbf{W}^{-1}\delta\mathbf{x}\right\|_2^2$. Multiplying both sides of the inequality by ξ and taking the square root of the resulting expression completes the proof. □

This theorem may be viewed an extension of IV.1 such that with a given $\mathbf{K}$, $\mathbf{W}$, $\gamma_i, i \in \mathcal{N}_{n_p}$, the transient bound ξ may be minimized by solving SDPs.

C. Control Synthesis with Harmonic Excitation Inputs

In order to apply the transient bound result of Lemma IV.1 to the closed-loop dynamics with harmonic dynamics in Section III.C, a slight modification is required. The additional harmonic states are accounted for explicitly within the following theorem.

Theorem IV.2. *Consider the closed-loop system described by* (30)*,* (31)*, and* (32)*, where the perturbations satisfy the norm bounds* $\|p_i\|_2 \leq \gamma_i \|\mathbf{v}_i\|_2$*,* $i \in \mathcal{N}_{n_p}$*. Let* $\mathbf{W} > 0$ *and* $r > 0$ *be chosen such that* $\mathbb{X}_c = \mathcal{E}_{n_x}(\mathbf{W}) \subseteq \mathbb{X}$ *and* $\mathbb{U}_c = r\mathcal{B}_{n_u} \subseteq \mathbb{U}$*, respectively. Then, the harmonic-embedded closed-loop system described by* (30)*,* (31)*, and* (32) *is locally bounded as*

$$\left\|\mathbf{W}^{-1}\delta\mathbf{x}(T)\right\|_2^2 \leq \xi^2 \left(\left\|\mathbf{W}^{-1}\delta\mathbf{x}(0)\right\|_2^2 + \left\|\bar{\boldsymbol{\beta}}(0)\right\|_2^2\right) \tag{40}$$

if there exist $\mathbf{P} \in \mathbb{S}^{n_x}$*,* $\mathbf{K} \in \mathbb{R}^{n_u \times n_x}$*,* $\tau > 0$*, and* $\lambda_i > 0,\ i \in \mathcal{N}_{n_p}$*, such that* $\mathbf{P} > 0$*,*

$$\begin{bmatrix} \mathbf{P}(\mathbf{A}_s + \mathbf{A}_k) + (\mathbf{A}_s + \mathbf{A}_k)^\mathsf{T}\mathbf{P} & \mathbf{P}\hat{\mathbf{B}}_2 & \boldsymbol{\Theta} \\ \hat{\mathbf{B}}_2^\mathsf{T}\mathbf{P} & \boldsymbol{\Lambda} & \mathbf{0} \\ \boldsymbol{\Theta}^\mathsf{T} & \mathbf{0} & \boldsymbol{\Xi} \end{bmatrix} < 0, \tag{41}$$

$$\begin{bmatrix} \tau^2\mathbf{I} & \mathbf{K} \\ \mathbf{K}^\mathsf{T} & \mathbf{W}^{-1}\mathbf{W}^{-1} \end{bmatrix} \geq 0, \tag{42}$$

$$\tau + \psi \leq r, \tag{43}$$

$$\begin{bmatrix} \bar{\mathbf{W}}^\mathsf{T}\mathbf{P}\bar{\mathbf{W}} & \mathbf{C}_s^\mathsf{T} \\ * & \xi\mathbf{1} \end{bmatrix} \geq 0, \tag{44}$$

$$\bar{\mathbf{W}}^\mathsf{T}\mathbf{P}\bar{\mathbf{W}} - \xi\mathbf{1} \leq 0, \tag{45}$$

where $\boldsymbol{\Lambda} = -\mathrm{diag}\left(\lambda_1, \ldots, \lambda_{n_p}\right)$ *and* $\boldsymbol{\Xi} = -\mathrm{diag}(\frac{\lambda_1}{\gamma_1^2}\mathbf{I}, \ldots, \frac{\lambda_{n_p}}{\gamma_{n_p}^2}\mathbf{I}), \boldsymbol{\Theta} = [\lambda_1\boldsymbol{\Phi}_1, \ldots, \lambda_n\boldsymbol{\Phi}_{n_p}]$*, with* $\boldsymbol{\Phi}_i^\mathsf{T} = \mathbf{E}_i[\mathbf{C}_i + \mathbf{D}_i\mathbf{K} \quad \mathbf{D}_i\bar{\mathbf{T}}]$*,* $i \in \mathcal{N}_{n_p}$*,* $\bar{\mathbf{W}} = \mathrm{diag}(\mathbf{W}, \mathbf{1})$ *and* $\mathbf{C}_s = [\mathbf{1}_{n_x \times n_x}\ \mathbf{0}_{n_x \times 2n_h}]$*. The variable* $\psi = \max(|h|)$ *encapsulates the maximum magnitude of the harmonic wave.*

Proof. The proof follows the proof of Theorem 3.1 in [8] with some modification. Defining the non-negative function $V = \mathbf{z}^\mathsf{T}\mathbf{P}\mathbf{z}, \mathbf{P} > 0$, taking its time derivative, and using (30) yields

$$\dot{V} = \begin{bmatrix} \mathbf{z} \\ \mathbf{p} \end{bmatrix}^\mathsf{T} \begin{bmatrix} \mathbf{P}\mathbf{A}_s + \mathbf{A}_s^\mathsf{T}\mathbf{P} + \mathbf{P}\mathbf{B}_s + \mathbf{A}_k^\mathsf{T}\mathbf{P} & \mathbf{P}\hat{\mathbf{B}}_2 \\ * & \mathbf{0} \end{bmatrix} \begin{bmatrix} \mathbf{z} \\ \mathbf{p} \end{bmatrix}. \tag{46}$$

The inputs and outputs of each Δ_i can be rewritten as

$$\begin{bmatrix} \mathbf{v} \\ p_i \end{bmatrix} = \begin{bmatrix} \mathbf{E}_i \begin{bmatrix} (\mathbf{C}_{3,i} + \mathbf{D}_{3,i}\mathbf{K}) & \mathbf{D}_{3,i}\bar{\mathbf{T}} \end{bmatrix} & \mathbf{0} \\ \mathbf{0} & \mathbf{1}_i^\mathsf{T} \end{bmatrix} \begin{bmatrix} \mathbf{z} \\ \mathbf{p} \end{bmatrix} = \begin{bmatrix} \boldsymbol{\Phi}_i^\mathsf{T} & \mathbf{0} \\ \mathbf{0} & \mathbf{1}_i^\mathsf{T} \end{bmatrix} \begin{bmatrix} \mathbf{z} \\ \mathbf{p} \end{bmatrix}. \tag{47}$$

With knowledge that $p_i^2 \leq \gamma_i^2 \|\mathbf{v}_i\|_2$ is true point-wise in time for each $\Delta_i, \in \mathcal{N}_{n_p}$, this inequality can be written as

$$\begin{bmatrix} \mathbf{v}_i \\ p_i \end{bmatrix}^\mathsf{T} \begin{bmatrix} \gamma_i^2\mathbf{1} & \mathbf{0} \\ \mathbf{0} & -1 \end{bmatrix} \begin{bmatrix} \mathbf{v}_i \\ p_i \end{bmatrix} \geq 0. \tag{48}$$

To ensure that $\delta\mathbf{u} = \mathbf{K}\delta\mathbf{x} \in \mathbb{U}_c$ such that $\|\delta\mathbf{u}\|_2 \leq \tau$ and knowing $\left\|\mathbf{W}^{-1}\delta\mathbf{x}\right\|_2 \leq 1$ for all $\delta\mathbf{x} \in \mathbb{X}_c$ yields

$$\|\delta\mathbf{u}\|_2 = \|\mathbf{K}\delta\mathbf{x}\|_2 = \left\|\mathbf{K}\mathbf{W}\mathbf{W}^{-1}\delta\mathbf{x}\right\|_2 \tag{49}$$

$$\leq \bar{\sigma}(\mathbf{K}\mathbf{W}) \left\|\mathbf{W}^{-1}\delta\mathbf{x}\right\|_2 \leq \bar{\sigma}(\mathbf{K}\mathbf{W}) \tag{50}$$

where this can be equivalently expressed as $\tau^2\mathbf{1} \geq \mathbf{K}\mathbf{W}\mathbf{W}\mathbf{K}^\mathsf{T}$ and applying a Schur complement leads to (42). The next equation (43) constrain the control effort and harmonic signal is within the sampling size of r.

Returning to the norm bound of $\Delta_i, i \in \mathcal{N}_{n_p}$, multiplying both sides of (48) by (47) yields

$$\begin{bmatrix} \mathbf{z} \\ \mathbf{p} \end{bmatrix}^\mathsf{T} \begin{bmatrix} \gamma_i^2 \mathbf{\Phi}_i \mathbf{\Phi}_i^\mathsf{T} & \mathbf{0} \\ \mathbf{0} & -\mathbf{1}_i \mathbf{1}_i^\mathsf{T} \end{bmatrix} \begin{bmatrix} \mathbf{z} \\ \mathbf{p} \end{bmatrix} \geq 0. \tag{51}$$

Applying the Schur complement to (41) results in

$$\begin{bmatrix} \mathbf{P}\mathbf{A}_s + \mathbf{A}_s^\mathsf{T}\mathbf{P} + \mathbf{P}\mathbf{B}_s + \mathbf{A}_k^\mathsf{T}\mathbf{P} & \mathbf{P}\hat{\mathbf{B}}_2 \\ * & \mathbf{\Lambda} \end{bmatrix} - \begin{bmatrix} \mathbf{\Theta} \\ \mathbf{0} \end{bmatrix} \mathbf{\Xi}^{-1} \begin{bmatrix} \mathbf{\Theta} \\ \mathbf{0} \end{bmatrix}^\mathsf{T} < 0, \tag{52}$$

which can be equivalently written as

$$\begin{bmatrix} \mathbf{P}\mathbf{A}_s + \mathbf{A}_s^\mathsf{T}\mathbf{P} + \mathbf{P}\mathbf{B}_s + \mathbf{A}_k^\mathsf{T}\mathbf{P} & \mathbf{P}\hat{\mathbf{B}}_2 \\ * & \mathbf{\Lambda} \end{bmatrix} - \sum_{i=1}^{n_p} \begin{bmatrix} -\lambda_i \mathbf{\Phi}_i \frac{\gamma_i^2}{\lambda_i} \mathbf{\Phi}_i^\mathsf{T} \lambda_i & \mathbf{0} \\ \mathbf{0} & \mathbf{0} \end{bmatrix} < 0. \tag{53}$$

Multiplying (53) on the left and right by $\begin{bmatrix} \mathbf{z}^\mathsf{T} & \mathbf{p}^\mathsf{T} \end{bmatrix}$ and $\begin{bmatrix} \mathbf{z}^\mathsf{T} & \mathbf{p}^\mathsf{T} \end{bmatrix}^\mathsf{T}$, then substituting in (46) results in

$$\dot{V} + \sum_{i=1}^{n_p} \lambda_i \begin{bmatrix} \mathbf{z} \\ \mathbf{p} \end{bmatrix}^\mathsf{T} \begin{bmatrix} \gamma_i^2 \mathbf{\Phi}_i \mathbf{\Phi}_i^\mathsf{T} & \mathbf{0} \\ \mathbf{0} & -\mathbf{1}_i \mathbf{1}_i^\mathsf{T} \end{bmatrix} \begin{bmatrix} \mathbf{z} \\ \mathbf{p} \end{bmatrix} < 0. \tag{54}$$

Knowing that $\lambda_i > 0, i \in \mathcal{N}_{n_p}$ and the inequality in (51) is satisfied, the S-procedure [15] implies that $\dot{V} < 0$.

Integrating $\dot{V} < 0$ from $t = 0$ to $t = T$, where $T \in \mathbb{R}_{>0}$, yields $V(T) \leq V(0)$ or $\mathbf{z}(T)^\mathsf{T}\mathbf{P}\mathbf{z}(T) \leq \mathbf{z}(0)^\mathsf{T}\mathbf{P}\mathbf{z}(0)$. Applying the non-strict Schur complement, (44) can be rewritten as $\xi^{-1}\bar{\mathbf{W}}^{-\mathsf{T}}\mathbf{C}_s^\mathsf{T}\mathbf{C}_s\bar{\mathbf{W}}^{-1} \leq \mathbf{P}$. The constraint (45) can be rewritten as $\mathbf{P} \leq \xi\bar{\mathbf{W}}^{-\mathsf{T}}\bar{\mathbf{W}}^{-1}$. Combining these results yields

$$\xi^{-1}\mathbf{z}(T)^\mathsf{T}\bar{\mathbf{W}}^{-\mathsf{T}}\mathbf{C}_s^\mathsf{T}\mathbf{C}_s\bar{\mathbf{W}}^{-1}\mathbf{z}(T) \leq \mathbf{z}(T)^\mathsf{T}\mathbf{P}\mathbf{z}(T) \leq \mathbf{z}(0)^\mathsf{T}\mathbf{P}\mathbf{z}(0) \leq \xi\mathbf{z}(0)^\mathsf{T}\bar{\mathbf{W}}^{-\mathsf{T}}\bar{\mathbf{W}}^{-1}\mathbf{z}(0). \tag{55}$$

Substituting $\bar{\mathbf{W}} = \mathrm{diag}(\mathbf{W}, \mathbf{1})$ and $\mathbf{C}_s\bar{\mathbf{W}}^{-1} = \begin{bmatrix} \mathbf{W}^{-1} & \mathbf{0} \end{bmatrix}$ into (55), then multiplying by ξ results in

$$\delta\mathbf{x}(T)^\mathsf{T}\mathbf{W}^{-\mathsf{T}}\mathbf{W}^{-1}\delta\mathbf{x}(T) \leq \xi^2 \left(\delta\mathbf{x}(0)^\mathsf{T}\mathbf{W}^{-\mathsf{T}}\mathbf{W}^{-1}\delta\mathbf{x}(0) + \bar{\boldsymbol{\beta}}(0)^\mathsf{T}\bar{\boldsymbol{\beta}}(0) \right), \tag{56}$$

which completes the proof. □

The result of Theorem IV.2 forms the basis of the proposed control synthesis method. Unfortunately, the constraints of (41)-(45) cannot be solved as an SDP, as they include bilinear matrix inequalities in variables $\mathbf{P}$, $\mathbf{K}$, τ, ξ and $\lambda_i, i \in \mathcal{N}_{n_p}$. To overcome this, the constraints are reformulated and/or relaxed into convex constraints that can be solved as SDPs for controller synthesis. Sections IV.D and IV.E present the relaxations needed to formulate the proposed iterative convex control synthesis method.

D. Control Synthesis via Relaxation

A key convex relaxation that is implemented for the purposed of control synthesis is the restriction that $\mathbf{P}$ be block diagonal (i.e., $\mathbf{P} = \mathrm{diag}(\mathbf{P}_{11}, \mathbf{P}_{22})$ where $\mathbf{P}_{11} \in \mathbb{S}^{n_x}$ and $\mathbf{P}_{22} \in \mathbb{S}^{2n_h}$). The inverse of $\mathbf{P}$ is thus also block diagonal, $\mathbf{R} = \mathbf{P}^{-1} = \mathrm{diag}(\mathbf{R}_{11}, \mathbf{R}_{22})$ where $\mathbf{R}_{11} = \mathbf{P}_{11}^{-1}$ and $\mathbf{R}_{22} = \mathbf{P}_{22}^{-1}$. Applying a congruence transformation on (41) with $\mathrm{diag}(\mathbf{P}^{-1}, \mathbf{1})$, then using the change of variables $\mathbf{R} = \mathbf{P}^{-1}$ and $\mathbf{F} = \mathbf{K}\mathbf{R}_{11}$ yields

$$\begin{bmatrix} \mathbf{A}_s\mathbf{P}^{-1} + \mathbf{P}^{-1}\mathbf{A}_s^\mathsf{T} + \mathbf{A}_k\mathbf{P}^{-1} + \mathbf{P}^{-1}\mathbf{A}_k^\mathsf{T} & \hat{\mathbf{B}}_3 & \mathbf{P}^{-1}\mathbf{\Theta} \\ * & \mathbf{\Lambda} & \mathbf{0} \\ * & * & \mathbf{\Xi} \end{bmatrix} < 0 \tag{57}$$

$$\begin{bmatrix} \mathbf{A}_s\mathbf{R} + \mathbf{R}\mathbf{A}_s^\mathsf{T} + \mathbf{A}_k\mathbf{R} + \mathbf{R}\mathbf{A}_k^\mathsf{T} & \hat{\mathbf{B}}_3 & \tilde{\mathbf{\Theta}} \\ * & \mathbf{\Lambda} & \mathbf{0} \\ * & * & \mathbf{\Xi} \end{bmatrix} < 0, \tag{58}$$

where $\tilde{\mathbf{\Theta}} = \begin{bmatrix} \lambda_1 \tilde{\mathbf{\Phi}}_1 & \dots & \lambda_{n_p} \tilde{\mathbf{\Phi}}_{n_p} \end{bmatrix}$, $\tilde{\mathbf{\Phi}}_i^\mathsf{T} = \mathbf{E}_i \begin{bmatrix} \mathbf{C}_{3,i}\mathbf{R}_{11} + \mathbf{D}_{3,i}\mathbf{F} & \mathbf{D}_{3,i}\bar{\mathbf{T}}\mathbf{R}_{22} \end{bmatrix}$, $i \in \mathcal{N}_{n_p}$, and $\mathbf{A}_k\mathbf{R} = \text{diag}(\mathbf{BF}, \mathbf{0})$.

Another relaxation is defined by setting $\lambda_i = \lambda$ and applying a congruence transformation of $\text{diag}(\sqrt{\lambda}\mathbf{1}, \frac{1}{\sqrt{\lambda}})$ as well as the coordinate transformations $\bar{\mathbf{R}} = \lambda\mathbf{R}$, $\bar{\mathbf{F}} = \lambda\mathbf{F} = \mathbf{K}\bar{\mathbf{R}}_{11}$. This yields

$$\begin{bmatrix} \lambda(\mathbf{A}_s\mathbf{R} + \mathbf{R}\mathbf{A}_s^\mathsf{T} + \mathbf{A}_k\mathbf{R} + \mathbf{R}\mathbf{A}_k^\mathsf{T}) & \hat{\mathbf{B}}_3 & \bar{\mathbf{\Theta}} \\ * & \mathbf{1} & \mathbf{0} \\ * & * & \bar{\mathbf{\Xi}} \end{bmatrix} < 0 \tag{59}$$

$$\begin{bmatrix} \mathbf{A}_s\bar{\mathbf{R}} + \bar{\mathbf{R}}\mathbf{A}_s^\mathsf{T} + \mathbf{A}_k\bar{\mathbf{R}} + \bar{\mathbf{R}}\mathbf{A}_k^\mathsf{T} & \hat{\mathbf{B}}_3 & \bar{\mathbf{\Theta}} \\ * & \mathbf{1} & \mathbf{0} \\ * & * & \bar{\mathbf{\Xi}} \end{bmatrix} < 0, \tag{60}$$

where $\bar{\mathbf{\Theta}} = [\bar{\mathbf{\Phi}}_1 \ \dots \ \bar{\mathbf{\Phi}}_{n_p}]$, $\bar{\mathbf{\Phi}}_i^\mathsf{T} = \mathbf{E}_i[\mathbf{C}_{3,i}\bar{\mathbf{R}}_{11} + \mathbf{D}_{3,i}\bar{\mathbf{F}} \ \ \mathbf{D}_{3,i}\bar{\mathbf{T}}\bar{\mathbf{R}}_{22}]$, $\mathbf{A}_k\bar{\mathbf{R}} = \text{diag}(\mathbf{B}\bar{\mathbf{F}}, \mathbf{0})$ and $\bar{\mathbf{\Xi}} = -\text{diag}(\frac{1}{\gamma_1^2}\mathbf{1}, \dots, \frac{1}{\gamma_n^2}\mathbf{1})$.

The LMIs of (58) and (60) are convex relaxations of the bilinear matrix inequality in (41) that are used to develop the proposed iterative convex control synthesis method described in Section IV.F. Any solutions to the LMIs of (58) and (60) are ensured to satisfy the bilinear matrix inequality of (41).

E. Controller Size Relaxation

Due to the change of variables and congruence transformations applied to (41) in Section IV.D, a corresponding change needs to be performed on (42) for use within the proposed control synthesis method. First, a congruence transformation with $\text{diag}(\mathbf{1}, \mathbf{R}_{11})$ is applied to (42) and the change of variables $\epsilon = \sqrt{\tau}$ and $\mathbf{F} = \mathbf{K}\mathbf{R}_{11}$ are made, yielding

$$\begin{bmatrix} \varepsilon\mathbf{I} & \mathbf{F} \\ \mathbf{F}^\mathsf{T} & (\mathbf{W}^{-1}\mathbf{R}_{11})^\mathsf{T}(\mathbf{W}^{-1}\mathbf{R}_{11}) \end{bmatrix} \geq 0, \tag{61}$$

which is a bilinear matrix inequality with respect to $\mathbf{R}_{11}$ and ensures that $\bar{\sigma}(\mathbf{KW}) \leq \sqrt{\varepsilon}$. Using the completion of squares identity $\mathbf{X}^\mathsf{T}\mathbf{Y} + \mathbf{Y}^\mathsf{T}\mathbf{X} \leq \mathbf{X}^\mathsf{T}\mathbf{X} + \mathbf{Y}^\mathsf{T}\mathbf{Y}$ for $\mathbf{X}, \mathbf{Y} \in \mathbb{S}^{n_x}$ and setting $\mathbf{Y} = \mathbf{1}$, $\mathbf{X} = \mathbf{W}^{-1}\mathbf{R}_{11}$ [14, 16], allows for the LMI

$$\begin{bmatrix} \varepsilon\mathbf{I} & \mathbf{F} \\ \mathbf{F}^\mathsf{T} & (\mathbf{W}^{-1}\mathbf{R}_{11})^\mathsf{T} + (\mathbf{W}^{-1}\mathbf{R}_{11}) - \mathbf{1} \end{bmatrix} \geq 0, \tag{62}$$

to be formulated, which implies the bilinear matrix inequality in (61).

Alternatively, a different relaxation of the bilinear term $(\mathbf{W}^{-1}\mathbf{R}_{11})^\mathsf{T}(\mathbf{W}^{-1}\mathbf{R}_{11})$ for a given $\mathbf{R}_{11}$ can be performed by linearizing the bilinear term about a feasible $\mathbf{R}_{11_0}$, which is similar to the convex overbounding approach in [17]. We do this by setting $\mathbf{X} = \mathbf{W}^{-1}\mathbf{R}_{11}$ and $\mathbf{Y} = \mathbf{W}^{-1}\mathbf{R}_{11_0}$ within the completion of the squares identity to yield the LMI

$$\begin{bmatrix} \varepsilon\mathbf{I} & \mathbf{F} \\ \mathbf{F}^\mathsf{T} & \mathbf{T}_1 \end{bmatrix} \geq 0, \tag{63}$$

where $\mathbf{T}_1 = (\mathbf{W}^{-1}\mathbf{R}_{11})^\mathsf{T}(\mathbf{W}^{-1}\mathbf{R}_{11_0}) + (\mathbf{W}^{-1}\mathbf{R}_{11_0})^\mathsf{T}(\mathbf{W}^{-1}\mathbf{R}_{11}) - (\mathbf{W}^{-1}\mathbf{R}_{11_0})^\mathsf{T}(\mathbf{W}^{-1}\mathbf{R}_{11_0})$.

Finally, to express (42) in terms of the variables $\mathbf{K}$ and $\mathbf{P}$, instead of $\mathbf{F}$ and $\mathbf{R}$, we perform a congruence transformation with $\text{diag}\,(\mathbf{I}, \mathbf{P}_{11})$ and then a Schur complement to obtain

$$\begin{bmatrix} \varepsilon\mathbf{I} & \mathbf{K} & \mathbf{0} \\ \mathbf{K}^\mathsf{T} & \mathbf{T}_2 & \mathbf{P}_{11} \\ \mathbf{0} & \mathbf{P}_{11} & \mathbf{R}_{11_0}^{-1}\mathbf{W}\mathbf{W}\mathbf{R}_{11_0}^{-1} \end{bmatrix} \geq 0, \tag{64}$$

where $\mathbf{T}_2 = \mathbf{W}^{-1}\mathbf{W}^{-1}\mathbf{R}_{11_0}\mathbf{P}_{11} + \mathbf{P}_{11}(\mathbf{W}^{-1}\mathbf{R}_{11_0})^\mathsf{T}\mathbf{W}^{-1}$.

F. Iterative Control Synthesis Algorithm

Theorem IV.2 along with the relaxations presented in Sections IV.D and IV.E are used to formulate the following proposed iterative controller synthesis method.

1) Initialize $\mathbf{W}$, r, $\mathbf{\Pi}$ and $\mathbf{E}_i, i \in \mathcal{N}_{n_p}$ to compute $\mathbb{X}_c = \mathcal{E}_{n_x}(\mathbf{W})$ and $\mathbb{U}_c = r\mathcal{B}_{n_u}$. Compute $\bar{\mathbf{S}}$ and $\bar{\mathbf{T}}$ given the frequency and amplitude of the expected harmonic excitation signals.
2) Compute samples $p_i = \Delta_i(\mathbf{x}, \mathbf{u})$ for $\mathbf{x} \in \mathbb{X}_c$ and $\mathbf{u} \in \mathbb{U}_c$ to compute the norm bounds $\gamma_i, i \in \mathcal{N}_{n_p}$ that satisfy (48).
3) Set γ_i to a very small value and solve for a feasible $\mathbf{R}$, $\mathbf{F}$ and ε that satisfies the constraints (60), (62), $\mathbf{R} > 0$, and $\varepsilon > 0$. If no feasible solution is found, return to Step 1) to adjust $\mathbf{W}$, r and/or $\mathbf{\Pi}$. Otherwise, set $\mathbf{K} = \mathbf{F}\mathbf{P}_{11}$.
4) Set $\mathbf{P}_0 = \mathbf{W}^{-1}$ and use $\mathbf{K}$ to solve for a feasible $\mathbf{P}$, ε and $\lambda_i, i \in \mathcal{N}_{n_p}$ subject to (41), (64), $\mathbf{P} > 0$, $\varepsilon > 0$ and $\lambda_i > 0, i \in \mathcal{N}_{n_p}$. If no feasible solution is found, return to Step 1) to adjust $\mathbf{W}$, r and/or $\mathbf{\Pi}$. Otherwise, set $\mathbf{R}_0 = \mathbf{P}^{-1}$.
5) Fix $\mathbf{R}_0$ and solve for $\mathbf{R}$, ε subject to (58), (63), $\mathbf{R} > 0$, $\varepsilon > 0$ that minimizes ε. If no feasible solution is found, return to Step 1) to adjust $\mathbf{W}$, r and/or $\mathbf{\Pi}$. Otherwise, set $\mathbf{K} = \mathbf{F}\mathbf{P}_{11}$.
6) If the stopping criteria (43) is met, minimize ξ subject to (41), (64), (44), (45), $\mathbf{P} > 0$, $\lambda_i > 0, i \in \mathcal{N}_{n_p}$, then exit. Otherwise, return to Step 4).

Although this iterative control synthesis algorithm is similar in nature to the control synthesis method presented in [8], two key differences include 1) a guaranteed bound on the norm of the system state that must hold point-wise in time, which ensures that the system does not leave the sampled region of the state-space and 2) exogenous harmonic excitation signals are accounted for by the inclusion of internal harmonic dynamics.

V. Numerical Example

Numerical simulations are performed with the nonlinear hypersonic vehicle longitudinal model described in Section III.A. Numerical results in this section are presetned for scenarios with and without external harmonic signals to the elevator angle, δ_e. The trim condition with states $V_0 = 9962$ft/s, $\alpha_0 = 2.3^o$, $\theta_0 = 0.9768^o$ and $Q_0 = 0$ and inputs $\delta_{e0} = 13^o$ and $\Phi = 0.1294$ is chosen.

The nonlinearities of the control-oriented modelare characterized by the following functions

$$\mathbf{f}_1 = \frac{1}{m} T(\alpha, \Phi) \cos\alpha \mathbf{1}_1, \tag{65}$$

$$\mathbf{f}_2 = \frac{-1}{m} D(V, \alpha) \mathbf{1}_1, \tag{66}$$

$$\mathbf{f}_3 = -g \sin(\theta - \alpha) \mathbf{1}_1, \tag{67}$$

$$\mathbf{f}_4 = \dot{\alpha} \mathbf{1}_2, \tag{68}$$

$$\mathbf{f}_5 = \dot{Q}(V, \alpha, \delta_e, \Phi) \mathbf{1}_4, \tag{69}$$

such that $\mathbf{f} = \sum_i^{n_p} \mathbf{f}_i$, as described in (10).The sampling region of $\mathbb{X}_c \times \mathbb{U}_c$ is defined as $\mathbb{X}_c = \mathcal{E}(\mathbf{W})$, with $\mathbf{W} = \text{diag}(50, 0.05, 0.05, 0.05)$ and $\mathbb{U}_c = r\mathcal{B}$ with $r = 0.161$. In this numerical example, the sampling of $\Delta_i, i \in \mathcal{N}_{n_p}$ is computed from the analytic control-oriented model in (12), though the methodology allows for the incorporation of data from other sources, such as from a lookup table of CFD data. The weighting matrix $\mathbf{E}_i, i \in \mathcal{N}_{n_p}$ is chosen such that $\|\mathbf{v}_i\|_2 \leq 1, i \in \mathcal{N}_{n_p}$. The bounds computed for $\mathbf{\Lambda}$ are $\gamma_1^2 = 1.43682$, $\gamma_2^2 = 15.2734$, $\gamma_3 = 2.81978 \cdot 10^{-5}$, $\gamma_4^2 = 3.06664 \cdot 10^{-9}$ and $\gamma_5 = 0.00361895$.

A. Region of Attraction without Harmonic Excitation

Without the addition of any harmonic excitation signals, the sequential SDP synthesis method described in [8] is solved to obtain the controller. The transient bounds on the closed-loop response are then solved through the use of Lemma IV.1, which yields $\xi = 1.935$. This value of ξ that is larger than one implies that with this synthesized controller, while the states are guaranteed to converge to equilibrium from within $\mathbb{X}_c$, there is a possibility the states may stray outside of this set before returning back to $\mathbb{X}_c$. This unfortunately violates the sampling of $\Delta_i, i \in \mathcal{N}_{n_p}$, thus, invalidating the quantification norm bounds $\gamma_i, i \in \mathcal{N}_{n_p}$ and any guarantees of closed-loop stability. However, the insight provided by the transient bounds introduced in this work provide a guarantee that the states will remain within the sampled region, provided that the initial conditions are within the set $\mathbb{X}_\star \in \xi^{-1}\mathcal{E}(\mathbf{W}) = 0.5168\mathcal{E}(\mathbf{W})$. Local asymptotic stability is thus guaranteed for the region of attraction $\mathbb{X}_\star$ using the synthesized controller, which demonstrates the use of Lemma IV.1 as a tool for analysis purposes.

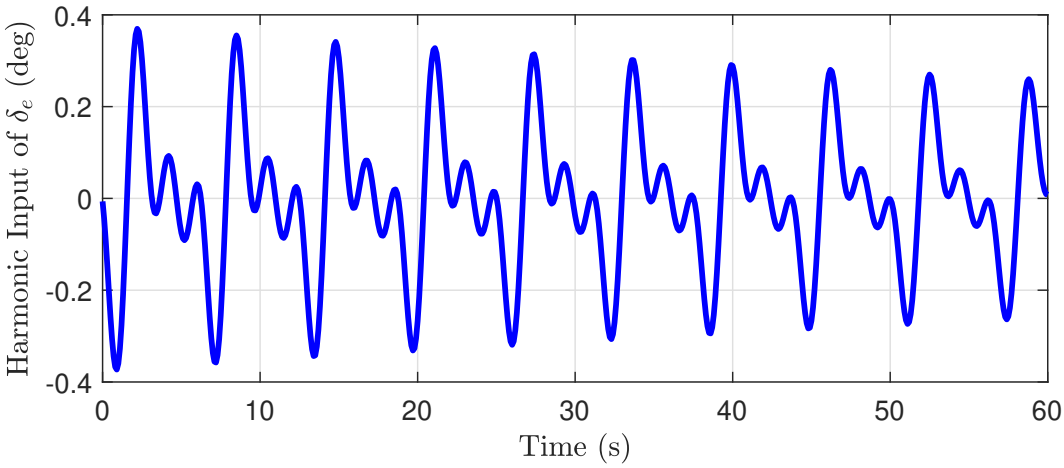

Fig. 3 The harmonic excitation signals applied to the closed-loop numerical simulations performed in Section V.B.

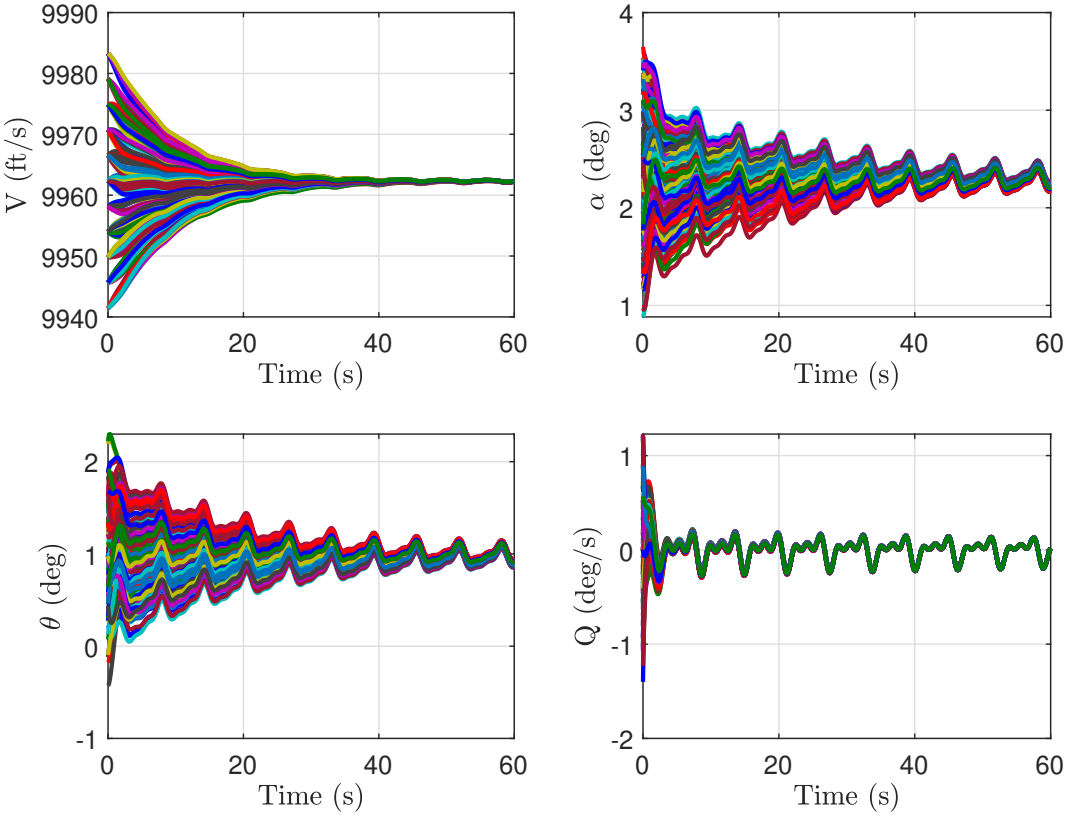

Fig. 4 Closed-loop results of the system states with 200 randomized sets of initial conditions from the numerical simulations performed in Section V.B.

B. Region of Allowable Initial Conditions with Harmonic Excitation

Three harmonic excitation signals with frequencies $\omega = \{1, 2, 3\}$ rad/s and amplitudes of $\delta_e = 0.15^o$ are added to the elevator input of the closed-loop system. The phase between the harmonic excirations are arbitrarily chosen as $\phi = \{-88.8085^o, -177.6169^o, -266.4254\}$ in the numerical results. Artificial damping of $\mu = 0.003$ is applied to force a small exponential decay of the harmonic signal. The resulting signal is shown Fig. 3 and represents the external harmonic excitation applied to the elevator angle input δ_e.

In Theorem IV.2, the bound on the region of allowable initial conditions $\mathcal{E}(\mathbf{W})$ depends not only on ξ, but also on

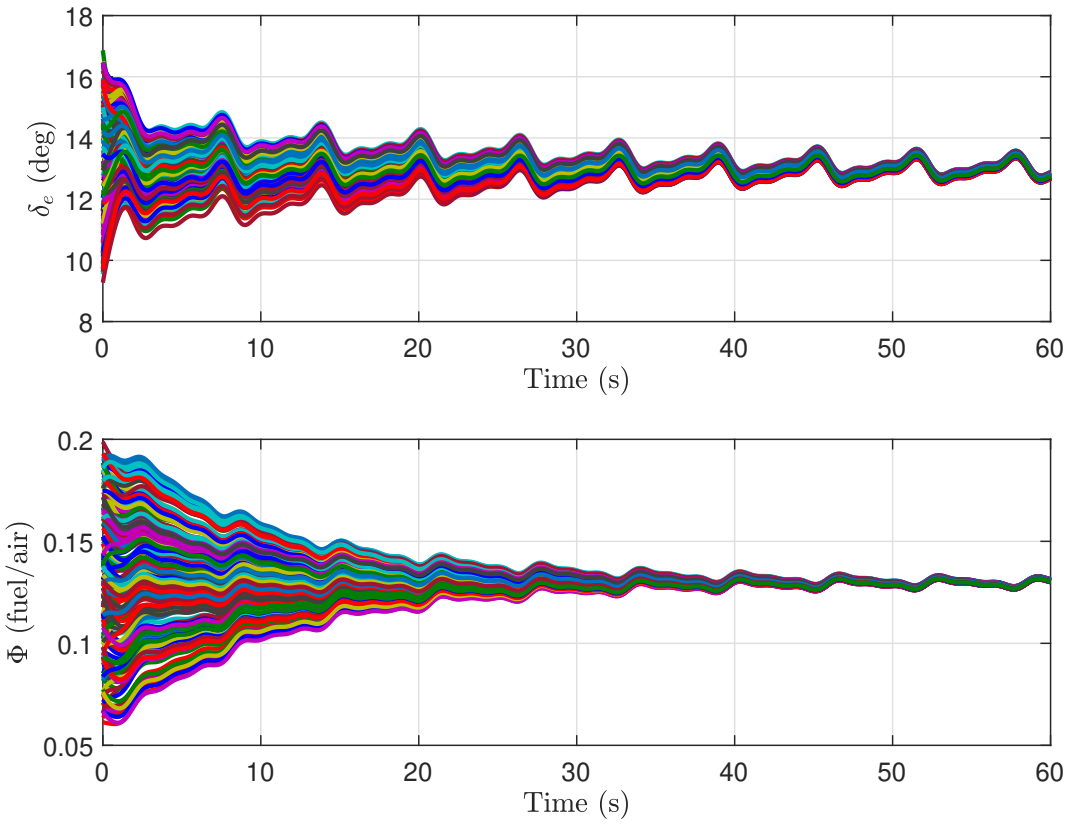

Fig. 5 Closed-loop results of the system inputs with 200 randomized sets of initial conditions from the numerical simulations performed in Section V.B.

$\bar{\boldsymbol{\beta}}(0)^\top \bar{\boldsymbol{\beta}}(0)$, indicating that the initial conditions of the harmonic signal plays a role in the bounding of the system states. By setting $\mathbf{\Pi} = 0.1 \cdot \max(\mathrm{diag}(\boldsymbol{\beta}))^{-1} = \mathrm{diag}(38.1972, 38.1972, 38.1972, 19.0986, 38.1972, 12.7324)$ for the change of coordinates, $\bar{\boldsymbol{\beta}}(0)^\top \bar{\boldsymbol{\beta}}(0) = 0.03$. This allows for tuning of the phase $\boldsymbol{\phi}$ to minimize ψ. The algorithm in Section IV.F is solved in MATLAB using `YALMIP` [18] and `MOSEK` [19], yielding a transient bound value of $\xi = 1.8824$ and the controller gain

$$\mathbf{K} = \begin{bmatrix} -0.0005 & 2.4608 & 0.5126 & 1.3894 \\ -0.0028 & 0.1242 & -0.9077 & -0.5698 \end{bmatrix}. \tag{70}$$

Substituting this and $\left\|\mathbf{W}^{-1}\delta\mathbf{x}(T)\right\|_2 = 1$ into (40), the region of allowable initial conditions is found to be $\mathbb{X}_{\star h} = 0.5022\mathcal{E}(\mathbf{W})$.

Numerical simulations are performed on the longitudinal hypersonic vehicle with 200 different randomized initial condition within the set $\mathbb{X}_{\star h}$ with the synthesized controller $\mathbf{K}$ and the harmonic excitation signal h applied to the elevator angle δ_e. The inputs from both the controller and the harmonic signal are shown in Fig. 5 where $\psi = 0.3723^o$. This value is accounted for in the constraint described by (43).

C. Discussion

In the scenario of no external harmonic excitations, the synthesized controller provides a guarantee of closed-loop asymptotic stability for the given region of attraction of $\mathbb{X}_\star = 0.5168\mathcal{E}(\mathbf{W})$, while still staying within bounds where the nonlinearities are adequately quantified through quadratic constraints. When an external harmonic excitation is present, asymptotic stability can no longer be guaranteed. Instead, a form of bounded output stability can be shown with the region of allowable initial conditions $\mathbb{X}_\star = 0.5022\mathcal{E}(\mathbf{W})$. This is slightly smaller than the previous scenario due to the need to account for the energy that the excitation signal adds to the system.

VI. Conclusions

This paper presented a control synthesis method that ensures boundedness of a nonlinear system's states in the presence of harmonic excitation inputs, with only input-output knowledge of the system's nonlinearities. This is an extension of the synthesis method presented in [8], which did not provide any transient bounds on the system's closed-loop response and did not account for any exogenous signals. The incorporation of transient bounds and hamornic excitation signals makes the proposed control synthesis amenable for hypersonic vehicle testing, as shown through numerical simulation results. When applied to a hypersonic vehicle prototype testing, our proposed method could allow for the vehicle to take on any harmonic excitation maneuvers within the boundary of $\mathcal{E}(\mathbf{W})$ and if for any reason this boundary is exceeded, the flight computer could switch to use the synthesized controller $\mathbf{K}$ to return to the flight trim condition. This could promote safe dynamic flight testing at the boundaries of the flight envelope, while to avoiding instability.

Future work will examine the means of maximizing the region of allowable initial conditions $\mathcal{E}(\mathbf{W})$ and a more automated way of choosing r, $\mathbf{E}_i$ and $\mathbf{\Pi}$ when no solution is found. Other methods of relaxing the bilinear matrix inequalities such as using penalty functions and parabolic relaxations will also be investigated as alternatives to the iterative method presented in this paper.

Acknowledgments

This material is based upon work supported by the Office of the Under Secretary of Defense for Research and Engineering under award number FA9550-21-1-0213. S.K. Cheah's contributions were partially supported by a University of Minnesota Informatics Institute MnDRIVE Ph.D. Graduate Assistantship. M.S. Hemati acknowledges partial support from the Air Force Office of Scientific Research under award numbers FA9550-21-1-0106 and FA9550-22-1-0004, the Army Research Office under award number W911NF-20-1-0156, and the National Science Foundation under award number CBET-1943988.

References

[1] Wang, Q., and Stengel, R. F., "Robust Nonlinear Control of a Hypersonic Aircraft," *Journal of guidance, control, and dynamics*, Vol. 23, No. 4, 2000, pp. 577–585. https://doi.org/10.2514/2.4580.

[2] Xu, H., Mirmirani, M. D., and Ioannou, P. A., "Adaptive sliding mode control design for a hypersonic flight vehicle," *Journal of Guidance, Control, and Dynamics*, Vol. 27, No. 5, 2004, pp. 829–838. https://doi.org/10.2514/1.12596.

[3] Keshmiri, S., Colgren, R., and Mirmirani, M., "Development of an aerodynamic database for a generic hypersonic air vehicle," *AIAA Guidance, Navigation, and Control Conference and Exhibit*, 2005, p. 6257. https://doi.org/10.2514/6.2005-6257.

[4] Gruhn, P., and Gülhan, A., "Aerodynamic measurements of an air-breathing hypersonic vehicle at Mach 3.5 to 8," *AIAA Journal*, Vol. 56, No. 11, 2018, pp. 4282–4296. https://doi.org/10.2514/1.J056522.

[5] Hou, Z.-S., and Wang, Z., "From model-based control to data-driven control: Survey, classification and perspective," *Information Sciences*, Vol. 235, 2013, pp. 3–35. https://doi.org/10.1016/j.ins.2012.07.014.

[6] Romer, A., Berberich, J., Köhler, J., and Allgöwer, F., "One-Shot Verification of Dissipativity Properties From Input–Output Data," *IEEE Contr. Syst. L.*, Vol. 3, No. 3, 2019, pp. 709–714. https://doi.org/10.1109/LCSYS.2019.2917162.

[7] Tanemura, M., and Azuma, S.-i., "Efficient data-driven estimation of passivity properties," *IEEE Contr. Syst. L.*, Vol. 3, No. 2, 2018, pp. 398–403. https://doi.org/10.1109/LCSYS.2018.2887241.

[8] Cheah, S. K., Bhattacharjee, D., Hemati, M. S., and Caverly, R. J., "Robust Local Stabilization of Nonlinear Systems with Controller-Dependent Norm Bounds: A Convex Approach with Input-Output Sampling," *IEEE Control Systems Letters*, Vol. 7, 2022, pp. 931–936. https://doi.org/10.1109/LCSYS.2022.3229004.

[9] Megretski, A., and Rantzer, A., "System analysis via integral quadratic constraints," *IEEE Transactions on Automatic Control*, Vol. 42, No. 6, 1997, pp. 819–830. https://doi.org/10.1109/9.587335.

[10] Parker, J. T., Serrani, A., Yurkovich, S., Bolender, M. A., and Doman, D. B., "Control-Oriented Modeling of an Air-Breathing Hypersonic Vehicle," *Journal of guidance, control, and dynamics*, Vol. 30, No. 3, 2007, pp. 856–869. https://doi.org/10.2514/1.27830.

[11] Bolender, M., and Doman, D., "A non-linear model for the longitudinal dynamics of a hypersonic air-breathing vehicle," *AIAA guidance, navigation, and control conference and exhibit*, 2005, p. 6255. https://doi.org/10.2514/6.2005-6255.

[12] Morelli, E. A., "Flight-test experiment design for characterizing stability and control of hypersonic vehicles," *Journal of Guidance, Control, and Dynamics*, Vol. 32, No. 3, 2009, pp. 949–959. https://doi.org/10.2514/1.37092.

[13] Zhou, K., *Robust and optimal control*, Prentice Hall, Englewood Cliffs, N.J., 1996.

[14] Caverly, R. J., and Forbes, J. R., "LMI Properties and Applications in Systems, Stability, and Control Theory," *CoRR*, Vol. abs/1903.08599, 2019. URL http://arxiv.org/abs/1903.08599.

[15] Boyd, S., El Ghaoui, L., Feron, E., and Balakrishnan, V., *Linear matrix inequalities in system and control theory*, SIAM, 1994.

[16] Zhou, K., and Khargonekar, P. P., "Robust stabilization of linear systems with norm-bounded time-varying uncertainty," *Systems & Control Letters*, Vol. 10, No. 1, 1988, pp. 17–20. https://doi.org/10.1016/0167-6911(88)90034-5.

[17] Warner, E., and Scruggs, J., "Iterative convex overbounding algorithms for BMI optimization problems," *IFAC PapersOnLine*, Vol. 50, No. 1, 2017, pp. 10449–10455. https://doi.org/10.1016/j.ifacol.2017.08.1974.

[18] Lofberg, J., "YALMIP: A toolbox for modeling and optimization in MATLAB," *2004 IEEE international conference on robotics and automation (IEEE Cat. No. 04CH37508)*, IEEE, 2004, pp. 284–289. https://doi.org/10.1109/CACSD.2004.1393890.

[19] ApS, M., *The MOSEK optimization toolbox for MATLAB manual. Version 9.0.*, 2019. URL http://docs.mosek.com/9.0/toolbox/index.html.